J. metamorphic Geol., 2007, **25,** 97–115 doi:10.1111/j.1525-1314.2006.00684.x

Experimental investigation of eclogite rheology and its fabrics at high temperature and pressure

J. ZHANG AND H. W. GREEN
Department of Earth Sciences and Institute of Geophysics and Planetary Physics, University of California, Riverside, CA 92521, USA (junfeng.zhang@email.ucr.edu)

ABSTRACT Eclogite plays an important role in mantle convection and geodynamics in subduction zones. An improved understanding of processes in the deeper levels of subduction zones and collision belts requires information on eclogite rheology. However, the deformation processes and associated fabrics in eclogite are not well understood. Incompatible views of deformation mechanism have been proposed for both garnet and omphacite. We present here deformation behaviour of eclogite at temperatures of 1027–1427 °C, confining pressures of 2.5–3.5 GPa, and strain rates of 1×10^{-5} s^{-1} to 5×10^{-4} s^{-1}. We obtained a power-law creep for the high temperature and pressure deformation of a 'dry' eclogite (50 vol.% garnet, 40% omphacite and 10% quartz) with $A = 10^{3.3 \pm 1.0}$, $n = 3.5 \pm 0.4$, $\Delta E = 403 \pm 30$ KJ mol^{-1} and $\Delta V = 27.2$ cm^3 mol^{-1}. The two principal minerals of eclogite have greatly different strengths. Progressive increase of garnet results in a smooth increase in strength. Analysis by electron back-scattered diffraction shows that: (1) garnet displays pole figures with near random distributions of misorientation angle under both dry and wet conditions; (2) omphacite shows pronounced lattice preferred orientations (LPOs), suggesting a dominant dislocation creep mechanism. Further investigation into the water effects on eclogite show: (3) water content does not influence the style of omphacite fabric but increases slightly the fabric strength; (4) grain boundary processes dominate the deformation of garnet under high water fugacity or high shear-strain conditions, yielding a random LPO similar to that of non-deforming garnet, despite the strong shape preferred orientation (SPO) observed. {110}[001] slip may dominate the deformation of rutile. Quartz displays complicated and inconsistent LPOs in eclogite. These results are remarkably similar to observations from deformed eclogites in nature.

Key words: deformation mechanism; eclogite; fabric; rheology.

INTRODUCTION

Eclogite, typically consisting of omphacite and garnet as the only major phases, is produced by crystallization of a basaltic melt at high pressure or by metamorphism of basalt or gabbro during subduction – in particular remnants of subducted oceanic crust (e.g. Ringwood & Green, 1966). Since its first introduction by Häuy (1822), eclogite has contributed to the birth of several major concepts in metamorphism and been involved in many geodynamic hypotheses during the last two centuries (Godard, 2001). Eclogitization of subducted oceanic crust during its reincorporation into the mantle is a critical part of the cycle of mantle convection that is still poorly understood. This eclogitization process and subsequent dehydration of alteration minerals accumulated while at the surface beneath the ocean have been cited as potentially involved in the generation of earthquakes (e.g. Austrheim & Boundy, 1994; Kirby *et al.*, 1996; Hacker *et al.*, 2003; Zhang *et al.*, 2004). Eclogite has been proposed to play an important role in the initiation of subduction and delamination of the continental crust (e.g. Bird, 1979; Kay & Kay, 1993; Seber *et al.*, 1996; Ducea & Saleeby, 1998) and of the subducting oceanic crust from the underlying lithosphere at both shallow and great depths (e.g. Sacks & Secor, 1990; Philippot & van Roermund, 1992; van Keken *et al.*, 1996; Warner *et al.*, 1996). Those processes depend critically on density contrast and flow property differences between eclogite and continental rocks and between eclogite and peridotite.

Eclogites also have been recognized as a reliable marker of ultrahigh-pressure (UHP) metamorphic environments in continental collision zones, with the key discoveries of coesite (e.g. Chopin, 1984; Smith, 1984) and microdiamonds (e.g. Sobolev & Shatsky, 1990; Xu *et al.*, 1992; Dobrzhinetskaya *et al.*, 1995) in deeply subducted crustal rocks, implying return to the surface from depths exceeding 120 km. Evidence is still accumulating that exhumation of rocks from even greater depths may occur in subduction terranes (e.g. Green *et al.*, 2000; Green, 2005). Little is currently understood of the processes responsible for such deep subduction and exhumation and the roles it may play in plate tectonics, continental growth, recycling of H_2O and other components back into the mantle, etc. In particular, eclogites may be a key repository of

information about these processes; they are more refractory than more silicic rocks, hence they are more likely to carry a 'memory' of their travels.

Extensive research has been conducted in the UHP metamorphic complexes of continental collision zones over the past two decades, with considerable focus on eclogites. Studies have included an extraordinary spectrum of topics and techniques including seismic surveys, geochronology, thermobarometry, the search for rare high-pressure minerals, geochemical investigations involving Raman and Infrared spectroscopies, determination of crystal structures and order/disorder phenomena, solid–solution ranges, exsolution processes, fluid and mineral inclusion identification, chemical zoning patterns and models of diffusion, element partition coefficients, stable isotope fractionations, REE patterns and investigation of deformation features such as dislocation mechanisms, microtextures and petrofabrics (for a small sample of these studies pertaining to eclogites, see Smith, 1988; Coleman & Wang, 1995; Hacker & Liou, 1998; Dobrzhinetskaya *et al.*, 2002). An improved understanding of tectonic processes in the deeper levels of subduction zones and collision belts requires information on the mechanical behaviour of eclogite; however, there have been no experimental studies of the rheology of eclogite except a preliminary experimental investigation of the flow of dry eclogite (Jin *et al.*, 2001) and announcement of discovery of a new faulting instability (Zhang *et al.*, 2004). It is therefore of great interest to explore in detail the deformation behaviour (rheological properties, deformation microstructure, deformation mechanism, etc.) of eclogite at high temperature and pressure.

In this paper, previous work on deformed eclogite, and its constituent minerals – garnet and omphacite – is first reviewed. Then, results of a systematic study of the rheology of a relatively 'dry' eclogite are presented, as well as effects of mineral fraction and water under a wide range of temperature, pressure and strain rate conditions. The fabrics of axially compressed and sheared eclogites are analysed by electron back-scattered diffraction (EBSD) to cast light on the deformation mechanisms in garnet, omphacite, quartz and rutile.

PREVIOUS STUDIES

Deformation of eclogite

Eclogite was not considered to be important in the mantle until the bloom of studies of eclogites in subduction zones and collision terranes two decades ago. Previously, eclogite was mostly studied from the mantle xenolith suite, in which they have largely been interpreted as high-pressure igneous crystallization products that have undergone little or no deformation. This interpretation, combined with the existing body of experimental evidence showing that garnet and pyroxene are very strong minerals, limited the interest in the study of the flow properties of eclogite. Eclogite is stable at pressures in excess of ~1.2 GPa. At temperatures sufficient for mineral reactions to proceed on a reasonable laboratory time-scale and to establish ductility of the constituent minerals (garnet and pyroxene), pressures in excess of 2 GPa are required, pressures outside the capacity of most conventional machinery designed to induce deformation and measure stresses (such as the Paterson apparatus and most Griggs deformation apparatus). No quantitative rheological data have been collected on eclogite except an early attempt at temperatures below 400 °C (Rummel, 1969). There are also no data on the flow properties of polycrystalline garnet and omphacite within the dislocation creep regime. The modified Griggs-type apparatus used here extends the range for controlled deformation experiments to 3.5–4.0 GPa.

As a consequence, understanding of eclogite rheology has been limited to inferences from microstructural observations and petrofabric measurements and sparse experimental studies on single crystals of garnet and pyroxene. Our previously reported preliminary experimental investigation of the rheology of dry eclogite has shown that eclogite has a strength comparable with that of harzburgite because of the weakness of omphacite, and garnet crystals behave essentially as rigid bodies in eclogite (Jin *et al.*, 2001). This result is in good agreement with inferences of many observations of naturally deformed eclogite (e.g. van Roermund & Boland, 1981; Godard, 1988; Godard & van Roermund, 1995). However, the deformation processes and associated fabrics in eclogite are not well understood. As is elaborated in detail below, incompatible views of deformation mechanisms have been proposed for both garnet and omphacite.

Deformation of garnet

Garnet is a major component of eclogite, and is also present throughout all but the upper ~60 km of the peridotitic upper mantle, becoming increasingly abundant in the transition zone between 410- and 660-km depths (e.g. Ringwood, 1991). Therefore, the physical properties of garnet have important effects on the rheology and dynamics of the subducted oceanic lithosphere, especially the oceanic crust (which becomes eclogite in the shallow mantle and becomes garnetite in the transition zone as the pyroxene is progressively dissolved into garnet). Previous transmission electron microscopy (TEM) studies on mantle garnet have shown evidence of plastic deformation by dislocation creep and were interpreted to indicate high ductility of garnet of ultra-deep origin (Ando *et al.*, 1993; Doukhan *et al.*, 1994; Prior *et al.*, 2000). However, it is more common to observe much lower dislocation densities in garnet (including majorite) than in coexisting minerals in both naturally and experiment-

ally deformed samples (e.g. Madon & Poirier, 1980; van Roermund, 1983; Ingrin & Madon, 1995). Quantitative studies of garnet creep have been very sparse. There exist only a limited number of experimental studies on plasticity of garnet (Karato *et al*., 1995; Cordier *et al*., 1996; Vöegele *et al*., 1998; Wang & Ji, 1999, 2000). Karato *et al*. (1995) conducted a series of studies on the plastic deformation of a suite of garnet single crystals at high temperature and room pressure. A unified rheological law for all the garnet studied was proposed. Their results showed that the resistance to plastic deformation in garnet is significantly higher than for other minerals in the Earth's mantle. They found the creep strength of garnet single crystals is largely controlled by the resistance to dislocation glide rather than by recovery processes. Similar results were achieved by Ji and colleagues. Wang & Ji (1999) extrapolated their results on garnet single crystals to natural conditions and estimated that garnet becomes ductile at around 800–900 °C and that the rheological contrast between garnet and clinopyroxene is minimal at temperatures higher than that. Cordier *et al*. (1996) and Vöegele *et al*. (1998) studied the plastic deformation of garnet single crystals under high confining pressure (6.5 GPa). They suggested brittle deformation of garnet below 1000 °C and ductile deformation above 1000 °C, characterized by dislocation creep with significant recovery. However, no correlation was found between dislocation microstructure and hydrous components in garnet.

Dislocation creep and diffusion creep of garnet have been argued for and supported by various pieces of evidence from previous studies. TEM studies revealed the long lengths of the dominant Burgers vector of garnet dislocations, $1/2<111>$ and $<100>$ (Allen *et al*., 1987). This, together with the high creep strength of garnet determined in the laboratory, has led to a generalized assumption that garnet remains essentially rigid during natural deformation (Karato *et al*., 1995). Garnet with strong shape preferred orientation (SPO) has been proposed to deform by grain boundary processes (e.g. den Brok & Kruhl, 1996; Terry & Heidelbach, 2004, 2006; Storey & Prior, 2005). However, discovery of dislocations in elliptically shaped garnet led to the opposite argument that garnet could deform by dislocation creep under high temperatures (Ji & Martignole, 1994; Ji *et al*., 2003). Recent EBSD studies revealed random distributions of crystallographic preferred orientation (lattice preferred orientations, LPO) of elliptical garnet from naturally deformed eclogites (e.g. Wenk *et al*., 2001; Storey & Prior, 2005). In contrast, weak LPO of flattened garnet were also documented in deformed granulites (Kleinschrodt & McGrew, 2000; Kleinschrodt & Duyster, 2002). Currently, little is still understood about how natural garnet is deformed and what mechanism dominates the deformation processes – dislocation creep, diffusion creep or grain boundary processes.

Deformation of omphacite

Omphacite is the other major constituent mineral in eclogite and it clearly has been extensively deformed in tectonic regimes. Deformation of omphacite at temperatures as low as 500–600 °C and a low flow strength compared with garnet was also suggested by microstructural observations (van Roermund & Boland, 1981; Philippot & van Roermund, 1992; Godard & van Roermund, 1995; Mauler *et al*., 2001). However, previous extensive studies have shown high strength for pyroxene (clinopyroxene: polycrystals: Avé Lallement, 1978; Kirby & Kronenberg, 1984; Boland & Tullis, 1986; single crystal: Raterron & Jaoul, 1991; orthopyroxene: polycrystals: Raleigh *et al*., 1971; Ross & Nielsen, 1978; single crystal: Mackwell, 1991). In marked contrast to these results, Stöckhert & Renner (1998) reported preliminary deformation experiments on synthetic polycrystalline jadeite (sodic clinopyroxene) aggregates at a pressure of 3.5 GPa and a temperature of 800–900 °C. Their data indicated a considerable strength difference between jadeite and diopside-hedenbergite clinopyroxene. They questioned the high strength that has been inferred for eclogites, which is also consistent with the microstructure of natural eclogites – in which omphacite with sutured grain boundaries forms an interconnected network around apparently rigid garnet. The recent experimental study on omphacite rheology of (Zhang *et al*. (2006) reached similar conclusions.

An LPO with [001] parallel to X (greatest elongation direction) and (010) parallel to the XY (foliation) plane was found to be common in omphacite of natural eclogites (e.g. van Roermund & Boland, 1981; Godard & van Roermund, 1995; Mauler *et al*., 2001; Bascou *et al*., 2002; Brenker *et al*., 2002; Ji *et al*., 2003). This pattern varies with the axial ratios of the shape fabric ellipsoid and can be divided into S- and L-type fabrics (Helmstaedt *et al*., 1972; Mauler *et al*., 2001). However, the identified dominant glide systems in clinopyroxene are (100)[001], {110}[001] and $\{110\}1/2<110>$ (van Roermund & Boland, 1981; van Roermund, 1983; Ingrin *et al*., 1991; Raterron *et al*., 1994). Because the (010)[001] slip system has not been reported as a dominant slip system in clinopyroxene, the observed omphacite fabrics cannot be explained by 'easy slip' on this slip system, resulting in a disconnect between submicroscopic observations and macroscopic fabrics. This has led to a debate over whether omphacite fabrics are formed by a single slip system or multiple slip systems (van Roermund, 1983; Buatier *et al*., 1991; Boundy *et al*., 1992; Bascou *et al*., 2001; Brenker *et al*., 2002). Other mechanisms, such as diffusion creep with concomitant anisotropic growth and dissolution, also have been argued to contribute to such fabrics (Helmstaedt *et al*., 1972; Godard & van Roermund, 1995; Mauler *et al*., 2001). Another unsolved question is the variation between L- and S-type fabrics. Omphacite space group

transformation (Brenker *et al*., 2002) and change of strain regime (Helmstaedt *et al*., 1972; Mauler *et al*., 2001) have been proposed for explanation of the fabric variation. The latter has been tested successfully with an anisotropic viscoplastic self-consistent model (Bascou *et al*., 2001, 2002). All of these questions remain to be answered by additional experimental work.

Water in eclogite

Water has been found to have a disproportionately large influence on the mechanical and physicochemical properties of silicates, such as lowering the solidus temperature (e.g. Green, 1973; Poli & Schmidt, 2002), reducing rheological strength (e.g. Griggs & Blacic, 1965; Griggs, 1967; Boland & Tullis, 1986), causing rock failure (e.g. Raleigh & Paterson, 1965; Jung *et al*., 2004; Zhang *et al*., 2004) and changing deformation fabrics (e.g. Jung & Karato, 2001). Trace amounts of hydroxyl (OH) have been detected spectroscopically in many nominally anhydrous minerals (e.g. Griggs & Blacic, 1965; Griggs, 1967; Bell & Rossman, 1992). Specifically, eclogites with non-trivial OH contents have been reported from both upper mantle (Aines & Rossman, 1984; Smyth *et al*., 1991) and UHP terranes (Langer *et al*., 1993; Katayama & Nakashima, 2003). The solubility of OH in nominally anhydrous minerals is pressure dependent (e.g. Ingrin & Skogby, 2000) and provides an alternative to hydrous minerals for carrying H_2O to great depth.

Towards a better understanding of deformation behaviour of eclogite under high temperature and pressure conditions, a systematic experimental investigation has been undertaken into the rheology and fabrics of eclogite at strain-rates of 1×10^{-5} s^{-1}–5×10^{-4} s^{-1}, pressures of 2.5–3.5 GPa and temperatures of 1027–1427 °C.

METHODS

Rheological experiments

The experimental starting materials of a 'dry' eclogite were prepared from fresh, coarse-grained, coesite-bearing eclogite of the Bixiling garnet peridotite–eclogite complex, Dabie Mountains, Central China (Jin *et al*., 2001). The natural eclogite was gently ground to disaggregate it into individual crystals. Mineral fractions were separated and individually ground to ensure that the particles were around 30–50 μm and then recombined into synthetic eclogite. The quartz grains are somewhat larger (50–100 μm), which should have negligible effect on the rheology of eclogite, given the small percentage of quartz present. The starting materials were analysed by using a microscope coupled to a Fourier Transform Infrared spectrometer at 3000–4000 cm^{-1} spectral range with resolution of 2 cm^{-1} by average 500 scans. The results showed that garnet and quartz had hydroxyl concentrations below the resolution of the spectrometer; omphacite contained about 100–200 p.p.m. hydroxyl, and rutile had up to 6000 p.p.m. hydroxyl (see the 'dry' eclogite in Table 1).

A procedure was devised whereby specimens were individually hot pressed in our modified 5-GPa Griggs apparatus. Prior to hot pressing, the dried, well-mixed powder was loaded and hand-compacted into a platinum capsule (3-mm inner diameter and roughly 9-mm length) with nickel foil disks placed within the capsule at the top and bottom of the specimen. A small alumina piston (3-mm diameter and ~1.4-mm length) was placed on top of the upper Ni foil and within the capsule to ensure a clean weld and to protect the sample from decomposition or melting during welding. Cesium chloride was cast between the encapsulated sample and nickel sleeve to serve as the confining medium, and the entire assembly was stored in a vacuum oven at 110 °C for ≥12 h before insertion into the high-pressure apparatus. All specimens were annealed (isostatically hot pressed) in the deformation apparatus at a pressure of 3 GPa and a temperature of 1027 °C for 12 h. After hot pressing, the samples remained straight and cylindrical in the middle of the nickel sleeve and the specimen length was reduced by 40–45% and diameter increased by ~5%. It is established that this procedure produces fully dense cylindrical polycrystalline specimens. Subsequent axial compression experiments were first annealed as

Table 1. Composition and water concentration of starting materials.

Material	Mineral	Chemistry	Volume%	OH concentration[b] (wt. p.p.m.)	Whole-rock (wt $\%H_2O$)
'Dry' eclogite	Garnet	$Pyr_{21}Alm_{18}Gro_{61}$	50	< 10	~0.01
	Omphacite[a]	$Di_{58}Jd_{42}$	40	100~250	
	Quartz		~10	< 10	
	Rutile		~0.5 ± 0.2	4000–6000	
'Wet' eclogite	Garnet	$Pyr_{23}Alm_{20}Gro_{57}$	50	0–300	~0.1
	Omphacite[a]	$Di_{59}Jd_{41}$	49	1000–1300	
	Kyanite		~1	Not determined	
	Rutile		~0.3 ± 0.2	6000–8000	

[a]The space group of omphacite is *C2/c*. [b]Water content was measured by a BRUKER A 590 microscope Fourier Transform Infrared Spectrometer at Department of Chemistry, University of California, Riverside, USA. The water content was calculated with the absorption coefficients in Bell *et al*. (1995) for garnet and omphacite and Hammer & Beran (1991) for rutile. Pyr, pyrope; Alm, almandine; Gro, grossular, Di, diopside; Jd, jadeite.

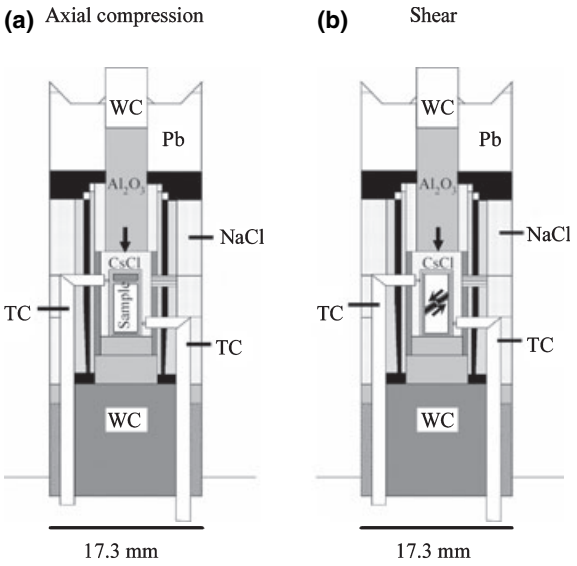

Fig. 1. Experimental assemblies viewed in cross section. (a) Assembly for axial compression experiments; (b) assembly for shear experiments. The specimen is welded into a platinum capsule, 9 mm × 3 mm, with a 1.4-mm high Al_2O_3 piston on top (axial compression) or between halves of a 9-mm Al_2O_3 piston cut at 45° in the middle. The capsule and surrounding sleeve of cesium chloride (CsCl) sit on a 2.5-mm high Al_2O_3 piston all within a thick nickel sleeve (Ni). CsCl also surrounds the upper Al_2O_3 deformation piston. The Ni sleeve on the inside and NaCl on the outside are insulated from the (tapered) graphite furnace (black) by fired pyrophyllite. Two $Pt_{90}Rh_{10}$-$Pt_{70}Rh_{30}$ thermocouples in mullite tubes, one at either end of the specimen, directly measure the axial temperature gradient during the experiment. WC – tungsten carbide; Pb = lead. Arrow in upper Al_2O_3 piston indicates method of deformation.

described and then subjected to constant piston velocity deformation (Fig. 1a).

About 20 axial compression experiments were undertaken to determine the flow law for 'dry' eclogite at 2.5–3.5 GPa and 1027–1427 °C (Table 2). The strain rates investigated overall fell in the range of 1×10^{-5}–5×10^{-4} s^{-1}. An additional ~10 axial compression experiments were conducted to investigate the effects of mineral fraction and water (Table 3). The latter includes a series of axial compression experiments on 'wet' eclogite containing up to 300 p.p.m. H_2O in garnet and 1000–1300 p.p.m. H_2O in omphacite (see the 'wet' eclogite in Table 1). Experiments were also carried out to investigate fabric development during high shear strain in 'dry' eclogite (Table 3). Specimens for high shear strain experiments were prepared by placing thin (~300-μm thick) slices of hot-pressed 'dry' eclogite between the halves of a 9-mm long Al_2O_3 rod cut at a 45° angle in the middle. They were then assembled for deformation runs like the axial compression experiments under similar *P–T* conditions (Fig. 1b).

All experiments were conducted in a 5-GPa modified Griggs-type apparatus (Tingle *et al.*, 1993). It has been shown that this apparatus provides accurate and precise rheological data at pressures up to 4.3 GPa (Bai & Green, 1998). The apparatus is equipped with a servo-controlled hydraulic drive and automated pressurization system. Data acquisition of pressure, load, temperature and displacement are also made through a computer. For the experiments described here, modifications were made to the sample assembly and graphite furnace to reduce the longitudinal temperature gradient typically to <15 °C over the specimen length; in exceptional circumstances, the temperature difference recorded by the two thermocouples differed during the experiment by as much as 30 °C.

Table 2. Experimental conditions and mechanical results of rheological experiments on 'dry' eclogite.

Expt No.	*P* (GPa)	*T* (°C)	$\dot{\varepsilon}$ (s^{-1})	Strain	σ (MPa)
GB190	3.0	1227	4.6×10^{-4}	37%	853
GB192	3.0	1327	4.6×10^{-4}	41%	413
GB193	3.0	1427	4.6×10^{-4}	45%	0 (molten)
GB194	3.0	1177	4.6×10^{-4}	24%	1175
GB200	3.0	1227	4.6×10^{-5}	18%	440
GB202	3.0	1227	1.3×10^{-4}	18%	500
GB203	3.0	1027	12-hour anneal		
GB209	3.0	1227	1.3×10^{-4}	14%	560
GB220	3.0	1277	4.6×10^{-4}	16%	559
GB242	3.0	1327	4.6×10^{-5}	32%	222
GB244	3.0	1327	1.3×10^{-4}	21%	323
GB246	3.0	1327	4.6×10^{-4}	25%	455
GB247	2.5	1227	4.6×10^{-4}	18%	565
GB249	3.5	1227	4.6×10^{-4}	19%	1010
GB252	2.6	1227	4.6×10^{-4}	23%	570
GB261	3.0	1177	4.6×10^{-5}	19%	650
GB263	3.0	1027	1.3×10^{-5}	23%	1019
GB267	3.0	1127	1.3×10^{-4}	25%	1102

Flow law: $\dot{\varepsilon} = 10^{3.3\pm1.0}\sigma^{3.5\pm0.4}\exp\left(\frac{-485\pm30\text{KJ/mol}}{RT}\right)$

EBSD analyses

Electron Back-Scattered Diffraction (EBSD) is an advanced technique for microstructure studies of metals and minerals in SEM. It is capable of determining the complete crystallographic orientation of individual grains or subgrains with a spatial resolution of ~1 μm and with an absolute angular resolution of ~1° (Prior, 1999). In principle, it is applicable to transparent and opaque crystalline solids of any crystal symmetry, including those that are optically isotropic. Thus, it provides a much more powerful tool than conventional universal-stage optical analysis, yielding more extensive and precise data obtained more quickly for study of LPOs in minerals and rocks.

For each specimen, a doubly polished thin section was cut parallel to the specimen axis. The section surface was polished with a 0.06-μm colloidal silica permanent suspension and then lightly carbon coated. The EBSD technique was used to measure the LPOs of omphacite and/or garnet in a Philips XL30 scanning electron microscope, using 20-kV accelerating voltage and 15-mm working distance with 70° tilting of thin sections. HKL CHANNEL 5 software was used to index electron back-scattered patterns. The reference

Expt. group	Expt. no.	Material[a]	T (°C)	$\dot{\varepsilon}$ (s^{-1})	Strain	σ (MPa)	H_2O (wt%)
Group I Composition effect	GB219	Omphacitite (0)	1254	4.6×10^{-4}	21%	307	0.02
	GB250	Eclogite (23)	1227	4.6×10^{-4}	16%	528	0.015
	GB190	Eclogite (50)	1227	4.6×10^{-4}	37%	853	0.01
	GB251	Eclogite (68)	1227	4.6×10^{-4}	16%	1148	0.005
	GB201	Garnetite (90)	1227	4.6×10^{-4}	< 10%	> 1746	< 0.001
	GB222	Harzburgite	1227	2.4×10^{-4}	12%	656	ND
Group II Water effect	GB224	Eclogite (50)	1227	4.6×10^{-4}	20%	402	2.7
	GB258	Eclogite (50)	1227	1.3×10^{-4}	39%	280	1.0
	GB275	Eclogite (50)	1227	4.6×10^{-4}	23%	761	0.1
	GB304	Eclogite (50)	1227	1.3×10^{-4}	13%	575	0.1
	GB284	Eclogite (50)	927	1.3×10^{-4}	31%	1572	0.1
Group III Shear expt.	GB320	Eclogite (50)	1227	[b]$2 \sim 4 \times 10^{-3}$	3.7	375	0.01
	GB321	Eclogite (50)	1127	[b]$2 \sim 5 \times 10^{-3}$	5.5	360	0.01

[a]The values in brackets are volume percentage of garnet in eclogite. [b]Constant piston advancing velocity is 0.6 μm s^{-1}. ND, not determined.

Table 3. Experimental conditions and mechanical results of comparison experiments.

coordinates (XYZ) were determined according to the deformation regime of individual experiments (axial compression: XY = normal to specimen long axis, Z = specimen long axis; simple shear: XY = shear plane, X = shear direction, Z = normal to shear plane). Pole figures were projected with equal area in the lower hemisphere and contoured with a half width of 20° and a cluster size of 5°. The orientation of each identified crystal in this study was collected and confirmed manually to ensure precision of measurements. Orientations of ~100–200 grains were collected for omphacite, quartz and rutile, while 200–300 orientation data were collected for garnet.

RESULTS

Deformation microstructures

Optical examination of the hot-pressed 'dry' eclogite specimens (Fig. 2a,b) showed well-equilibrated microstructures with dominant grain size of 30–50 μm for garnet and omphacite, and 50–100 μm for quartz. A weak foliation defined by slight flattening of quartz and omphacite perpendicular to the cylinder axis was observed. Optical microstructures of moderately deformed 'dry' eclogite specimens (Fig. 3a) show a strong foliation defined by obviously deformed omphacite and greatly elongated quartz. Undulatory extinction and subgrain boundaries are common in both omphacite and quartz grains. After 40–45% strain, quartz grains are up to 100–150-μm long, showing a characteristic aspect ratio of 1:3 to 1:5. In runs at 1027 °C, small amounts of recrystallization of quartz were observed and/or partial transformation to coesite. Omphacite crystals are up to 50–100-μm long with characteristic aspect ratio of 3:5 to 1:3. Garnet shows no obvious elongation and behaves like essentially rigid bodies within the matrix of elongated omphacite and quartz, a texture essentially identical to the 'dry' natural eclogite used to prepare the specimens and very similar to many other deformed natural eclogites (e.g. Godard, 1988; Mauler *et al.*, 2001; Piepenbreier & Stöckhert, 2001). In contrast to the typical deformation microstructure in moderately deformed 'dry' eclogite, the experimentally deformed 'wet' eclogite develops a distinct foliation defined by both flattened garnet and omphacite (Fig. 3b). High magnification images of the garnet in such specimens revealed clear evidence of recrystallization near the edge of crystals and apparent 'sliding off' of the new, small, garnet into the foliation (Fig. 3c). In high shear strain 'dry' experimental specimens, approximately monomineralic banding of garnet, omphacite and quartz is observed, together with significant grain size reduction of garnet (Fig. 3d). In some areas of these highly strained specimens, the garnet is strung out into the foliation, reminiscent of the small garnet 'sliding off' of large garnet in 'wet' eclogite. Thus, 'dry' specimens subjected to low-to-moderate strain, in which the garnet is widely separated from one another, show no deformation or recrystallization of garnet whereas at

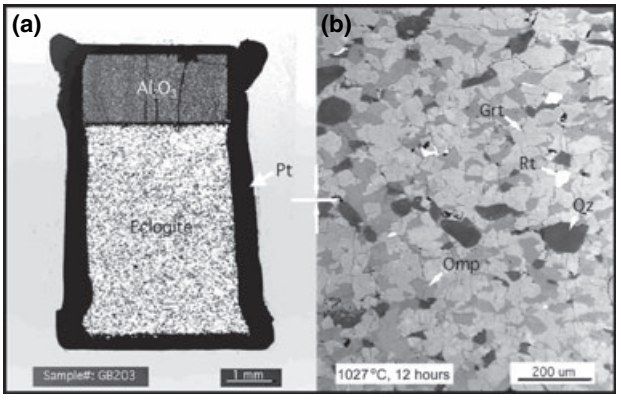

Fig. 2. Microstructures of synthetic eclogite (after Jin *et al.*, 2001). The part figure (a) shows that specimens remained approximately upright and retained cylindrical geometry after hot pressing at 3 GPa, 1027 °C for 12 h; The part figure (b) shows that specimens subjected only to pressurization and annealing developed a weak foliation defined by quartz and omphacite perpendicular to the cylinder axis – attributed to the ~40% uniaxial shortening imposed during pressurization (to remove porosity) followed by heating at high pressure (specimen GB203; (a), crossed polarizers; (b), reflected light).

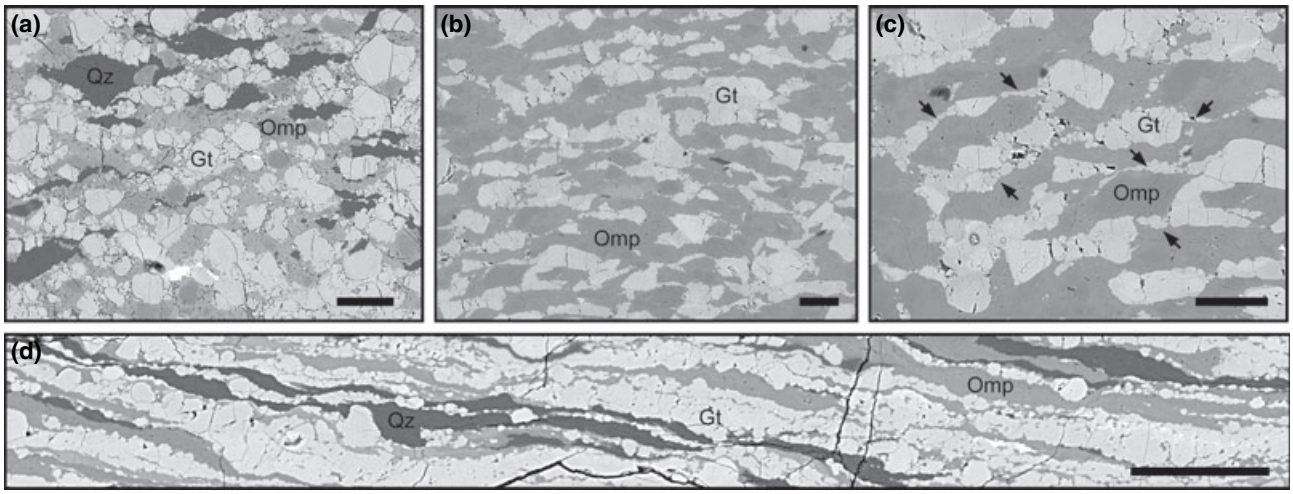

Fig. 3. Microstructures of experimentally deformed eclogites (the shortening direction is oriented N-S in panels a–c; the shearing direction is oriented E-W in panel d). Deformed experimental specimens developed a foliation defined by flattened omphacite and quartz grains in dry eclogite (a: specimen GB192) and a foliation defined by both flattened omphacite and garnet grains in wet eclogite (b: specimen GB275). Panel (c) shows a detail of flattened garnet in panel b; such garnet is made of a tail-like stream of recrystallized garnet flowing off rigid older garnet. Panel d shows highly elongated omphacite and quartz grains in a sheared specimen (GB321). Significant grain size reduction is observed in garnet. All panels are back-scattered electron SEM images of polished surfaces. Gt, garnet; Omp, omphacite; Qz, quartz; Ky, kyanite. Scale bars: 50 μm.

high strains, in which extreme deformation of quartz and omphacite have swept garnet together into garnetite bands, the same 'dry' material exhibits recrystallization similar to that shown in 'wet' specimens at low strains with widely separated garnet. We attribute the recrystallization of dry garnet to probable high local strains where garnet has been squeezed together, generating dislocations locally, a process that apparently occurs in 'wet' garnet in response to the much less severe local stresses caused by omphacite sliding across their surfaces. These deformation microstructures correspond closely to different types of deformation microstructures observed commonly in naturally deformed eclogite samples (e.g. Godard & van Roermund, 1995; Ji *et al*., 2003; Mainprice *et al*., 2004; Zhang & Green, 2006).

Experimental results

At high temperatures and pressures, plastic deformation of many materials often occurs by a power-law creep. The constitutive relation is well described by an empirical equation of form:

$$\dot{\varepsilon} = A\sigma^n \exp[-(Q/RT)], \qquad (1)$$

where A is the pre-exponential factor related with material, n is the stress exponent related to the deformation mechanism ($n = 3$–5 for dislocation creep and $n \sim 1$ for diffusion creep), $\dot{\varepsilon}$ is the strain rate, σ is the steady-state flow stress, R is the gas constant, T is the absolute temperature, $Q = \Delta G = \Delta H - T\Delta S$. ΔG is the activation Gibbs Free Energy, $\Delta H = \Delta E + P\Delta V$ is the activation enthalpy, and ΔE, ΔV, and ΔS are activation energy, activation volume and activation entropy, respectively (see Poirier, 1985; Green & Borch, 1987 for discussion of activation parameters).

To determine the rheological parameters for 'dry' eclogite at high pressure, several series of experiments at constant strain-rate or constant temperature were carried out at confining pressure of 2.5–3.5 GPa (Table 2). A first series of experiments was performed on eclogite at constant temperatures and different strain rates of 4.6×10^{-5} s^{-1}, 1.3×10^{-4} s^{-1} and 4.6×10^{-4} s^{-1}, respectively. A log-log plot of strain rate *v*. stress for those experiments is shown in Fig. 4(a), yielding a stress exponent, $n = 3.5 \pm 0.4$ and a pre-exponential factor, $A = 10^{3.3 \pm 1.0}$. A second series of experiments was carried out on eclogite at constant strain rates and different temperatures of 1177, 1227, 1277 and 1327 °C, respectively. A semi-log plot of strain rate *v*. inverse temperature is shown in Fig. 4(b), yielding an activation enthalpy, $\Delta H = 485 \pm 30$ KJ mol^{-1}. Optical microscopy showed that melting begins around 1327 °C at the grain boundaries of quartz and omphacite and progresses into the interior of omphacite grains and omphacite-garnet grain boundaries with increasing temperature. Experiment GB193 conducted at 1427 °C, showed no measurable flow stress and displayed 20 vol.% glass after quenching. A third group of eclogite experiments was conducted to assess the effect of pressure on flow strength at 1227 °C and 4.6×10^{-4} s^{-1}. A steady increase of flow strength with pressure was suggested with an activation volume of $\sim$27 cm^3 mol^{-1} (Fig. 4c). An increase of pressure of 1 GPa has approximately the same effect as an increase of temperature of 100 °C within the explored P–T window. Therefore, the acti-

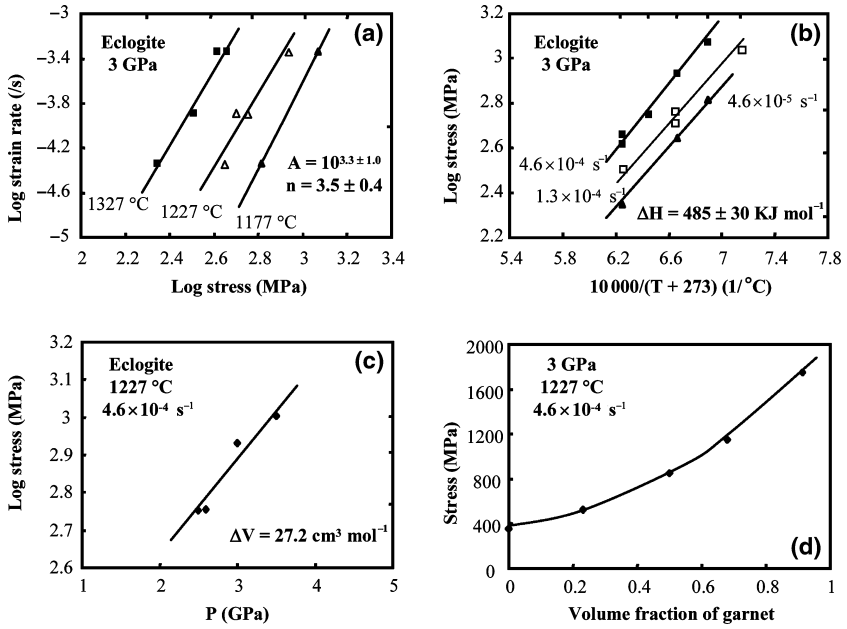

Fig. 4. Mechanical results of high temperature creep of eclogite. (a) Log-log plot of strain rate *v.* stress for steady-state flow of eclogite at 1177, 1227 and 1327 °C, respectively, yielding a stress exponent, $n = 3.5 \pm 0.4$. (b) Semi-log plot of strain rate *v.* inverse temperature for constant strain rate of 4.6×10^{-4} s^{-1}, 1.3×10^{-4} s^{-1} and 4.6×10^{-5} s^{-1}, respectively, yielding an activation enthalpy, $\Delta H = 485 \pm 30$ KJ mol^{-1}. (c) Semi-log plot of stress *v.* pressure for steady-state flow of eclogite at 1227 °C and 4.6×10^{-4} s^{-1}, yielding an activation volume of 27.2 cm^3 mol^{-1}. (d) Effect of garnet fraction on flow stress of eclogite showing a steady increase of eclogite strength with garnet content.

vation energy (ΔE) is estimated to be 403 ± 30 KJ mol^{-1}.

For comparison, several additional experiments were conducted under similar conditions (3 GPa, 4.6×10^{-4} s^{-1}, 1227 °C) on polycrystalline omphacite, polycrystalline garnet, intermediate compositions, harzburgite and 'wet' eclogite. These experiments yielded creep strengths of ~300 MPa for polycrystalline omphacite, >1746 MPa for polycrystalline garnet and ~650 MPa for harzburgite (Table 3, expt. Group I). A steady increase of eclogite flow strength with garnet content is indicated in Fig. 4(d). However, examination of the most garnet-rich samples after deformation generally showed that the alumina inner piston also was deformed, suggesting that the measurements of stress on the specimens of ~90% garnet may constitute only a lower bound on polycrystalline garnet strength. Adding H_2O to eclogite reduced the flow strength (Table 3, expt. Group II).

In summary, our results suggest that the two principal minerals of eclogite have greatly different strengths; the creep strength of 'dry' eclogite appears to be comparable with that of harzburgite within experimental error, but 2–3 times that of polycrystalline omphacite and no more than half that of polycrystalline garnet. Progressive increase of garnet fraction in the sample results in a smooth increase in strength. Water reduces the flow strength of eclogite as well as causes variation of the deformation microstructures.

EBSD ANALYTICAL RESULTS

Fabrics of hot-pressed 'dry' eclogite

Figure 5 shows representative LPOs of garnet, omphacite and quartz in a hot-pressed 'dry' eclogite. Our results show that garnet has a nearly random distribution of orientation with a narrow distribution density ranges [0.5–1.5 in multiples of random distribution (mrd)] (Fig. 5a,b). The misorientation angle distributions are also corresponding to theoretically random distributions (Fig. 5c). In contrast, a fairly weak S-type LPO is observed in omphacite: [001] axes form a broad girdle approximately parallel to the foliation; [010] axes are approximately normal to the foliation (Fig. 5d,e). Our results revealed also near random distribution fabrics in quartz (Fig. 5f,g).

Fabrics of compressed experimental 'dry' eclogite

The LPOs of all four minerals were analysed in our experimental 'dry' eclogites. These eclogites have been subjected to axial compression deformation under various temperature and strain rate conditions with limited strains (14–41%) as described in the previous section.

Figure 6 shows representative LPOs of garnet from four deformed dry eclogites as fabric diagrams of the <100>, <111> and <110> axes. All garnet pole figures have similar narrow distribution density ranges (0.5–1.5 in mrd) (Fig. 6a–h). The misorientation angle distributions are corresponding to theoretically random distributions (Fig. 6i–l). No correlation was found between garnet fabrics and changes of experimental conditions or the amount of plastic strain.

The LPOs of omphacite from eight deformed dry eclogites are plotted as fabric diagrams of poles of {110} as well as [100], [010] and [001] axes in Fig. 7. Our results show typical S-type fabrics of varying strength in omphacite: [001] axes form a girdle

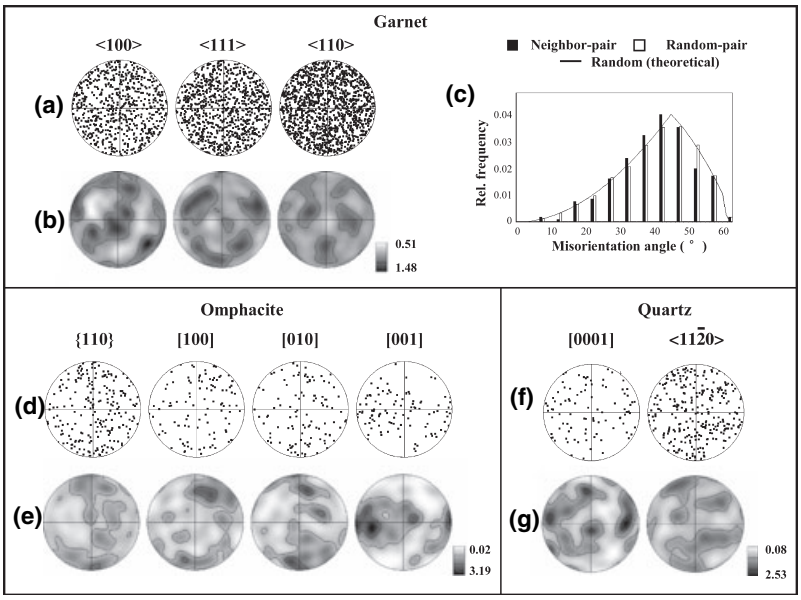

Fig. 5. Fabrics of garnet, omphacite and quartz in a typical hot-pressed 'dry' experimental specimen (GB203, 3 GPa, 1027 °C, 12-h cooking). Panels a and b are raw data and contoured lower-hemisphere equal-area projections of garnet lattice preferred orientations (LPO) expressed as $<100>$, $<111>$ and $<110>$ pole figures ($n = 217$ grains). Panel c is histogram of the relative frequency of misorientation angles. Black: misorientation data between neighbouring points; White: misorientation data between randomly chosen points; Curve: theoretical distribution from a random set of orientations. Panels d and e are contoured lower-hemisphere equal-area projections of omphacite LPO expressed as fabric diagrams of poles to {110} well as [100], [010] and [001] axes ($n = 108$ grains). Panels f and g are contoured lower hemisphere equal-area projections of quartz LPO expressed as fabric diagrams of the c[0001] axis and a $<11–20>$ axes ($n = 92$ grains). Half width, 20°; cluster size, 5°; grey scale, pole figure density (mrd).

approximately parallel to the foliation with multiple concentrations; poles of {110} and [010] axes are approximately normal to the foliation but the [010] fabric is more pronounced; [100] axes are relatively widely spread. They have small LS-indices between 0.153 and 0.415, confirming that they are S-type fabrics (see Ulrich & Mainprice, 2005 for introduction of LS-index). The causes of imperfection in these S-type fabrics can be attributed to slightly heterogeneous deformation and the relatively low accumulated strain. These results are also identical to the S-type omphacite fabrics of natural eclogites (e.g. Helmstaedt *et al.*, 1972). Variation of temperature or strain rate appears to have little effect on omphacite fabrics (Fig. 7a–h).

Although rutile is only an accessory mineral, it does show indications of plastic deformation in our experimentally deformed eclogites. Therefore, we managed to measure its fabrics from several samples in spite of its low abundance. Figure 8(a–c) shows representative LPOs of rutile from three experimentally deformed eclogites as fabric diagrams of the $<100>$, [001] axes and poles of {110}. A consistent fabric was found in rutile: [001] axes form a girdle approximately parallel to the foliation with multiple concentrations; [100] axes and poles of {110} are approximately normal to the foliation.

Quartz composes only 10% of the experimentally deformed specimens but shows the largest aspect ratio in its crystal shapes, implying that it has absorbed very large strains. Figure 8(d–i) shows representative LPOs of quartz from six deformed dry eclogite specimens as fabric diagrams of the **c**[0001] axis and **a** $<11–20>$ axes. Unlike all other minerals, our results revealed complicated and inconsistent fabrics in quartz throughout the studied samples.

Fabrics of compressed experimental 'wet' eclogite

The LPOs of garnet and omphacite in experimentally deformed 'wet' eclogites were investigated for comparison. These eclogites have been subjected to deformation with limited strains (23–31%) as described in detail in our eclogite faulting paper (Zhang *et al.*, 2004). Only those eclogite samples deformed without faulting were selected for EBSD analysis. Figure 9 shows two representative LPOs of garnet from experimentally deformed wet eclogites as fabric diagrams of the $<100>$, $<111>$ and $<110>$ axes. Random distributions of garnet orientation were also observed with a low-density range (0.6–1.4 in mrd) in spite of the strong SPO of garnet (Fig. 9a–d). The misorientation angle distributions also correspond to theoretically random distributions (Fig. 9e–f). The LPOs of omphacite from the same eclogites show the same S-type fabric in omphacite as those of experimentally deformed dry eclogites (Fig. 9g–j). Increasing the water content of omphacite by a factor of 10 caused no change on the style of omphacite fabric. However, the calculated LS-indices are relatively smaller than those of omphacite LPOs in dry eclogites, suggesting that water has facilitated the deformation of omphacite with better-oriented omphacite crystals relative to the macroscopic strain.

Fabrics of experimentally sheared 'dry' eclogite

The LPOs of garnet and omphacite from two experimentally sheared 'dry' eclogites were also analysed for comparison. These eclogites have been subjected to deformation under temperature and strain rate conditions comparable with the axial compression

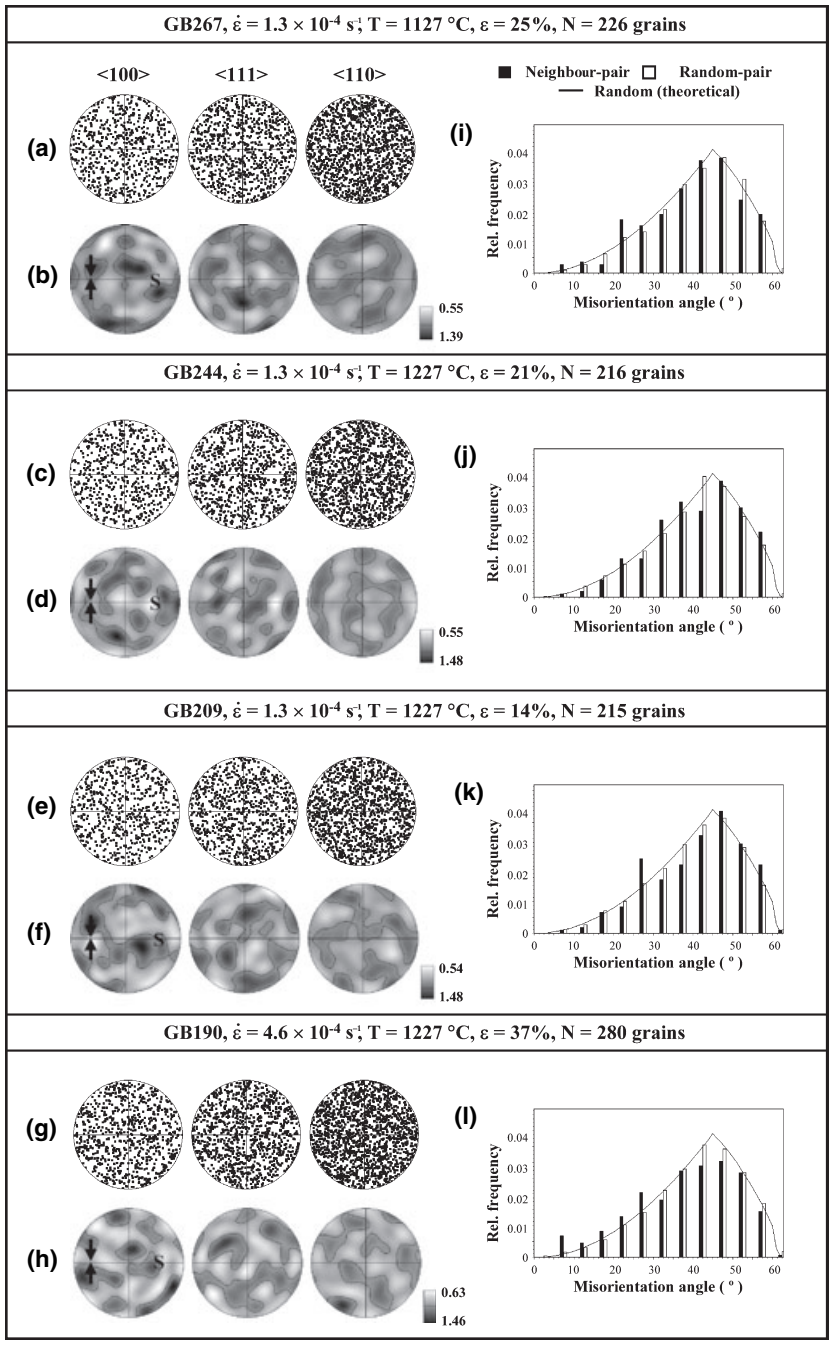

Fig. 6. Fabrics of garnet from four axially compressed experimental 'dry' eclogites. Panels a–h are raw data and contoured lower-hemisphere equal-area projections of garnet lattice preferred orientations expressed as $<100>$, $<111>$ and $<110>$ pole figures with half width of 20° and cluster size of 5°, respectively. Grey scale: pole figure density (mrd). S: foliation, vertical EW plane. Panels i–l are histograms of the relative frequency of misorientation angles. Black: misorientation data between neighboring points; White: misorientation data between randomly chosen points; Curve: theoretical distribution from a random set of orientations.

experiments but with large shear strains (γ = 3–6) (Table 3, expt. Group III). Figure 10 shows the LPOs of garnet as fabric diagrams of the $<100>$, $<111>$ and $<110>$ axes. Again a similar random distribution of garnet was observed with a low-density range (0.5–1.7 in mrd) (Fig. 10a–d). The misorientation angle distributions correspond to theoretically random distributions (Fig. 10e–f). No correlation was found between garnet fabric and changes of experimental conditions as well as the amount of strain. The LPOs of omphacite from these sheared eclogites show a strong LS-type fabric: [001] axes are near parallel to the shearing direction; [010] axes are normal to the foliation, poles of {110} concentrate at 45° to the foliation; [100] axes concentrate near the centre of the plot (Fig. 10g–j). Their corresponding LS-indices are 0.607–0.654, close to LS-indices (0.55–0.60) of typical LS-type fabrics of omphacite from VPSC simulations of simple and pure shear deformation (Ulrich & Mainprice, 2005). Thus, 'dry' deformation to very high strains, despite the obvious recrystallization of garnet (Fig. 3d), produces no

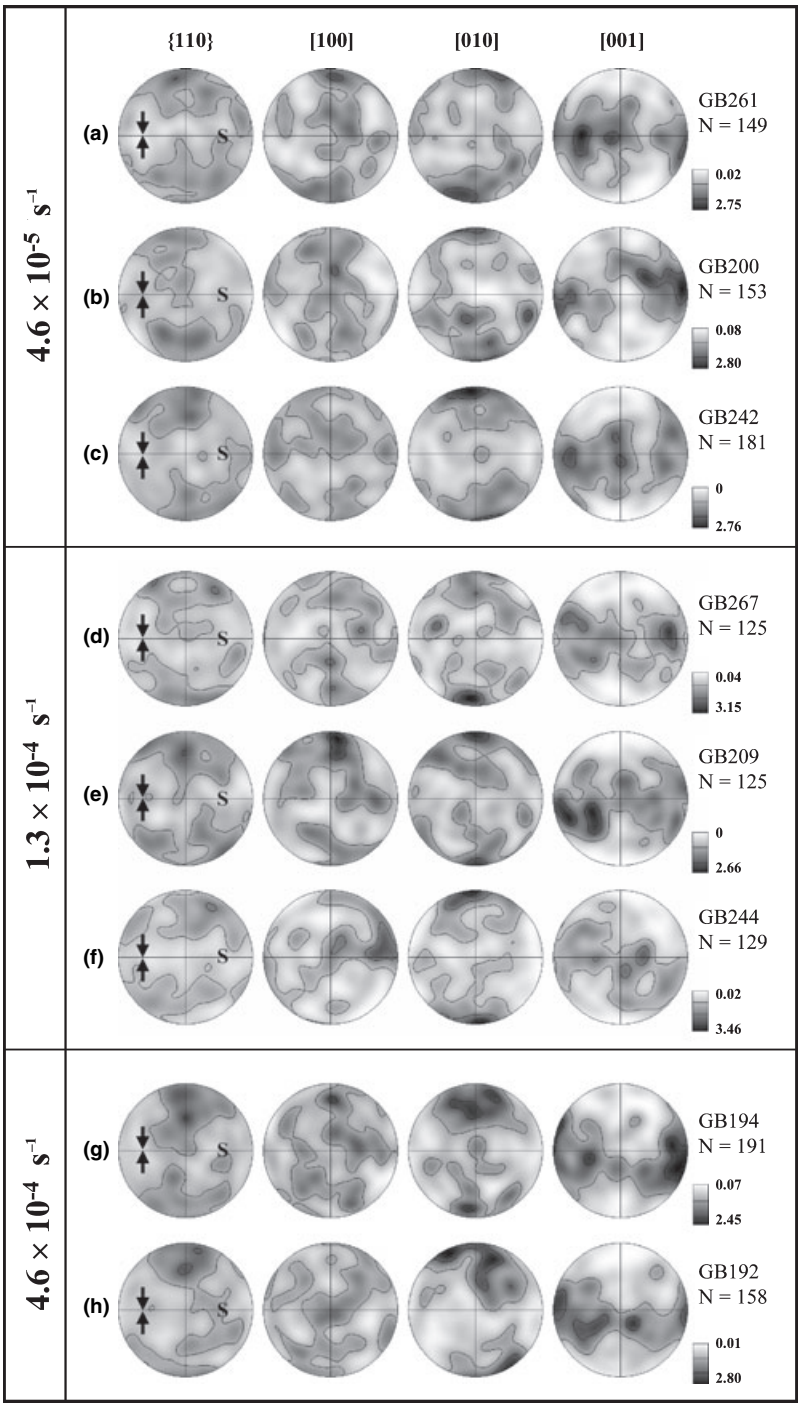

Fig. 7. Fabrics of omphacite from eight axially compressed experimental 'dry' eclogites. Panels a–h are contoured lower-hemisphere equal-area projections of omphacite lattice preferred orientations (LPO) expressed as fabric diagrams of poles to {110} as well as [100], [010] and [001] axes with half width of 20° and cluster size of 5°. They are typical S-type fabrics with small LS-indices (0.153–0.415). Grey scale: pole figure density (mrd). S: foliation, vertical EW plane. *N* is the number of measured grains.

LPO in garnet, exactly as was found for the recrystallization of garnet in 'wet' eclogite. We thus conclude that the recrystallization of garnet in both cases is driven by the same process, local plastic deformation imposed at the surfaces of the grains that results in rapid organization of dislocations into boundaries that then can readily slide and roll as strain progresses.

DISCUSSION

Eclogite rheology

Microstructural observations (flattened omphacite and quartz crystals, strong foliation, undulatory extinction, etc.) in the optical microscope and the measured stress exponent of $n = 3.5$ indicate that our experimental

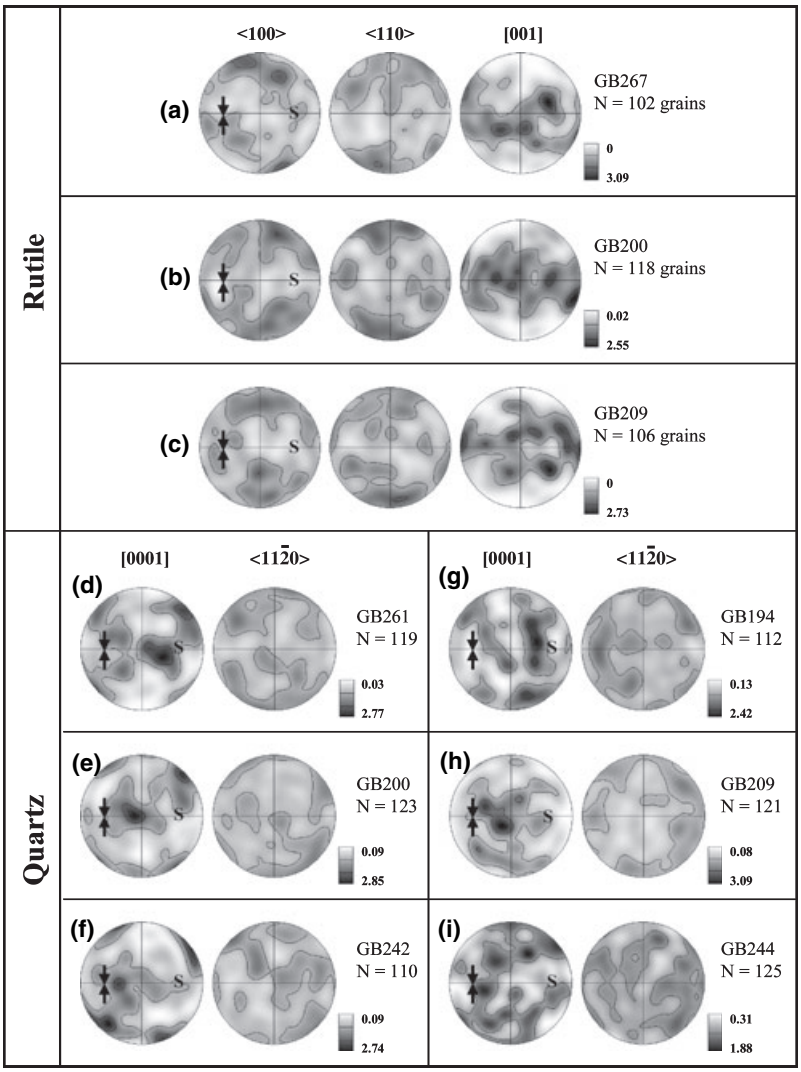

Fig. 8. Fabrics of rutile and quartz from axially compressed experimental 'dry' eclogites. Panels a–c are contoured lower-hemisphere equal-area projections of rutile lattice preferred orientations (LPO) expressed as fabric diagrams of the < 100 >, < 110 > and [001] axes with half width of 20° and cluster size of 5°. Panels d–i are contoured lower-hemisphere equal-area projections of quartz LPO expressed as fabric diagrams of the c[0001] axis and a < 11–20 > axes with half width of 20° and cluster size of 5°. Grey scale: pole figure density (mrd). S: foliation, vertical EW plane.

'dry' eclogite was deformed in the dislocation creep regime. The remarkable similarities of deformation microstructures and fabrics between the experimentally deformed samples and naturally deformed samples suggest that they have the same deformation mechanisms even though laboratory deformation is as much as 10 orders of magnitude faster than in nature. The deformation of 'dry' eclogite is accommodated by the weaker phases of omphacite and quartz so long as strains are sufficiently small that garnet does not collide; thus garnet behaves like rigid inclusions. This correlates with the pronounced omphacite fabric and a near random garnet fabric from the same eclogite. Experiments conducted separately on polycrystalline omphacite and garnet further demonstrate the great contrast in the creep strengths of these two minerals under both dry and wet conditions, and show that the strength of eclogite falls between the strengths of the end-member phases. The experiments on compositions of 23% and 68% garnet confirm the general trends.

Our data suggest that under comparable conditions omphacite is weaker than Ca-Mg clinopyroxene (Bystricky & Mackwell, 2001; Dimanov *et al*., 2003), but stronger than polycrystalline jadeite (sodic clinopyroxene) (Stöckhert & Renner, 1998), supporting the arguments of Stöckhert & Renner (1998) that sodic clinopyroxene could be weaker than Ca-Mg clinopyroxene (Zhang *et al*., 2006). Omphacite creep strength is also significantly lower than that of eclogite and close to that of wet clinopyroxenite, which suggests that regions in subducting slabs with significantly different ratios of garnet to omphacite will have strain partitioned into omphacite-rich domains. The weakness of omphacite also explains why eclogites from environments of 'UHP' metamorphism have experienced large deformations rather than remaining undeformed internally. The similarity in strength of eclogite and harzburgite as a consequence of the weakness of omphacite compensating for the high strength of garnet also resolves the contradiction between laboratory measurements on

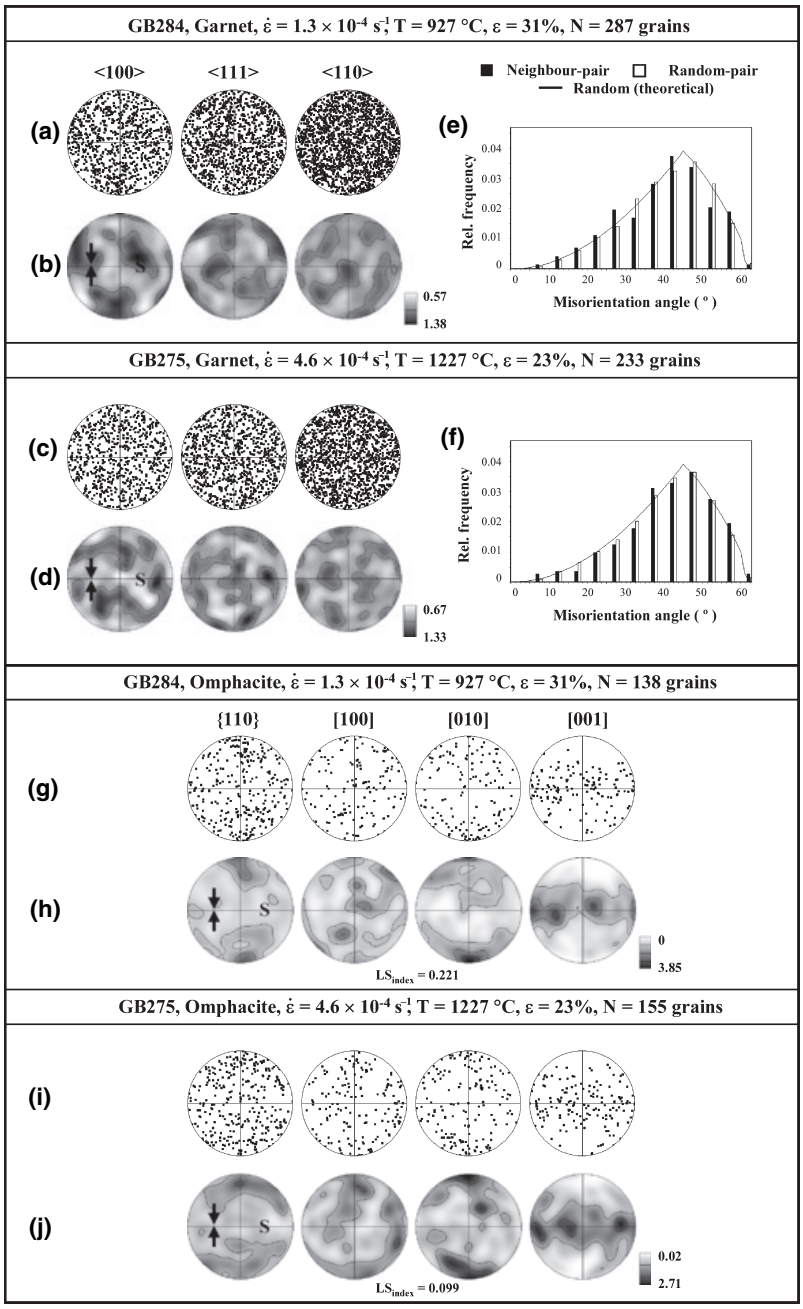

Fig. 9. Fabrics of garnet and omphacite from two representative axially compressed experimental 'wet' eclogites. Panels a–d are raw data and contoured lower-hemisphere equal-area projections of garnet lattice preferred orientations (LPO) expressed as fabric diagrams of the $<100>$, $<111>$ and $<110>$ directions with half width of 20° and cluster size of 5°, respectively. Panels e and f are corresponding histograms of the relative frequency of misorientation angles. Black: misorientation data between neighbouring points; White: misorientation data between randomly chosen points; Curve: theoretical distribution from a random set of orientations. Panels g–j are contoured lower hemisphere equal-area projections of omphacite LPO expressed as fabric diagrams of poles to {110} well as [100], [010] and [001] axes with half width of 20° and cluster size of 5°. Grey scale: pole figure density (mrd). S: foliation, vertical EW plane.

garnet and pyroxene and inferences made previously from studies of eclogites in subduction-zone complexes (e.g. van Roermund & Boland, 1981; Godard & van Roermund, 1995; Karato *et al*., 1995).

A significant decrease in creep strength and a pronounced change of deformation microstructure (elongated garnet crystals) has been observed in experimentally deformed eclogites because of the presence of water. Therefore, our data on the 'dry' eclogite provide only an upper bound for the rheology of eclogite. Natural sodic clinopyroxene commonly contains hundreds to thousands of p.p.m. hydroxyl in their structures while other pyroxene (diopside and enstatite) normally exhibit much less (tens to a few hundred p.p.m.) (Smyth *et al*., 1991; Katayama & Nakashima, 2003; Su *et al*., 2004). This difference may contribute partially to the low flow strength of sodic pyroxene as well as the chemical composition difference. It has also been shown recently that precipitation of water from such pyroxene induces melting at grain boundaries and causes high pressure faulting, which is a viable new mechanism for intermediate depth earthquakes within hot subducting oceanic crust (Zhang *et al*., 2004).

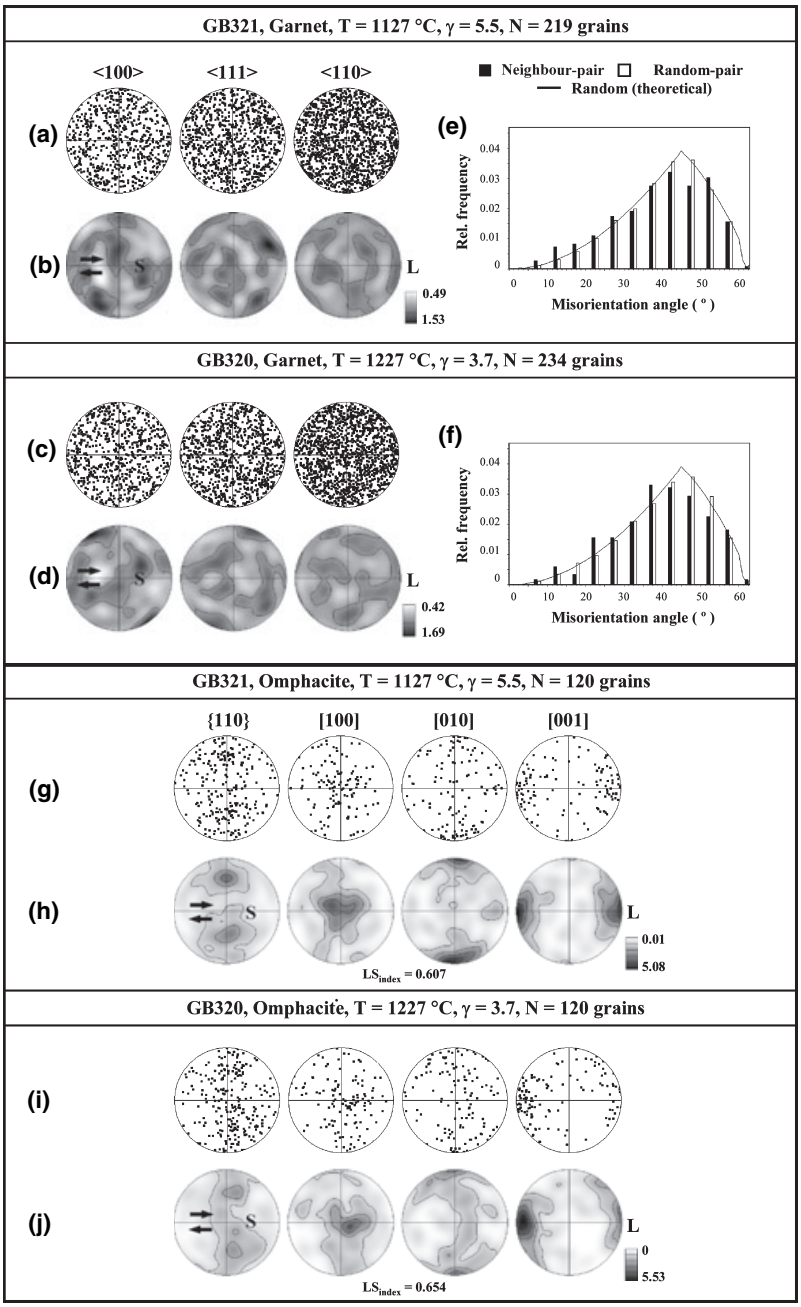

Fig. 10. Fabrics of garnet and omphacite from two representative sheared experimental 'dry' eclogites. The format is exactly the same as for Fig. 9. S: foliation, vertical EW plane; L: lineation, EW direction.

Deformation mechanism

Garnet deformation mechanism

The deformation mechanisms of natural garnet have been debated for years. The long Burgers vectors and high creep strength of garnet determined in the laboratory have led many to believe that garnet remains essentially rigid during deformation (e.g. Allen *et al.*, 1987; Karato *et al.*, 1995). This general assumption appears to explain very well subhedral-to-irregular garnet found in many crustal and mantle rocks (e.g. Godard, 1988). However, discoveries of some garnet with elliptical shapes challenged this argument and an opposite argument has been advanced that garnet could deform by dislocation creep under high temperatures despite the generally low density of dislocations in those garnet (Ando *et al.*, 1993; Doukhan *et al.*, 1994; Ji & Martignole, 1994; Ji *et al.*, 2003). In conflict to the latter argument are the weak or random LPOs of those elliptical garnet (Wenk *et al.*, 2001; Ji *et al.*, 2003; Storey & Prior, 2005). Numerical simulations of LPO development in garnet using the visco-plastic self-consistent model produce

strong characteristic LPOs for both axial compression and simple shear deformation (Mainprice *et al*., 2004). It is therefore difficult to explain weak garnet LPOs with dominant dislocation creep deformation, given the large plastic strain inferred from those elliptical garnet.

Our results appear to resolve this conflict. Firstly, the mechanical data confirm the great strength of garnet under dry conditions. Garnet is at least four-six times stronger than omphacite and twice as strong as harzburgite. It is therefore not surprising to find random LPOs in the round garnet from naturally and experimentally deformed dry eclogites. Secondly, our results demonstrate the great effect of water on deformation behaviour of garnet. Previous experimental study has shown that OH abundance in pyrope increases to 1000 p.p.m. at pressure of 5–7 GPa and then dehydrates at higher pressures (Withers *et al*., 1998). The discovery of high hydroxyl content and sodic amphibole exsolutions in garnet from UHP rocks provides evidence for the participation of water in the processes of garnet dynamics including deformation (Langer *et al*., 1993; Song *et al*., 2005). Our mechanical data suggest that trace amounts of structurally bonded hydroxyl may have a disproportionately large influence on the mechanical properties of garnet. Garnet shows indications of strong flattening in the experimental wet eclogite, indicating that the mechanical strength of garnet has been greatly reduced because of the presence of water in the system. However, EBSD analysis of those elongated garnet shows the same random LPOs as for garnet in the 'dry' eclogites. The analyses of natural elliptical eclogitic garnet yields similar results (Storey & Prior, 2005; Zhang & Green, 2006). The mismatch between LPO and SPO of 'wet' garnet suggests that intracrystalline dislocation creep did not dominate the deformation of garnet. Other mechanisms must be the cause of the elongated shape of garnet. Back-scattered imaging shows that natural lenticular garnet is often made of numerous subgrains, suggesting grain-boundary sliding processes assisted by subgrain formation and rotation have dominated the plastic deformation instead of dislocation creep (Storey & Prior, 2005; Zhang & Green, 2006). Similarly, we observed repeatedly apparent sliding off into the foliation of recrystallized superficial layers of experimental garnet in the experimental 'wet' eclogites (Fig. 3c), suggesting that the majority of strain in garnet is accomplished by grain-boundary sliding as well. Similar observations after very large strains imposed on 'dry' eclogite (Fig. 3d) suggest that the same process can operate in 'dry' eclogite, but only after extreme deformation of the weaker phases has brought garnet together and generated high local contact stresses.

In summary, it is clear that water causes significant changes in the flow properties of garnet in eclogite. Dry garnet is very strong and resistant to plastic flow at all temperatures examined here and can only flow after very large strains under conditions where recrystallization induces extensive grain-boundary sliding similar to that found in wet eclogites at smaller strains. No evidence was found of bulk dislocation flow of garnet either in experiments or in nature. In all cases, no garnet LPO develops, regardless of the amount of bulk strain.

Omphacite deformation mechanism

Our experiments have produced microstructures and deformation fabrics of omphacite remarkably similar to those found in natural eclogites, suggesting that they have the same deformation mechanisms even though laboratory deformation is as much as 10 orders of magnitude faster than in nature. Our experiments clearly are incompatible with diffusion creep based on the rheological measurements. Moreover, the presence of strong LPOs in omphacite lacking extensive recrystallization unambiguously indicates dislocation creep as the dominant deformation mechanism in the experimentally deformed eclogites. This mechanism also is in agreement with microstructural observations (flattened omphacite crystals, strong foliation, undulatory extinction, a high density and wide variety of dislocations, etc.) (Zhang *et al*., 2006).

As for naturally deformed eclogites, numerous previous studies have demonstrated that dislocation creep is a major deformation mechanism in omphacite (van Roermund & Boland, 1981; van Roermund, 1983; Godard & van Roermund, 1995; Brenker *et al*., 2002; Ji *et al*., 2003; Zhang *et al*., 2006). However, diffusion creep may occur in fine-grained omphacite as suggested by a few studies (Philippot & van Roermund, 1992; Godard & van Roermund, 1995; Mauler *et al*., 2001). Both mechanisms have been shown analytically capable to produce the observed omphacite LPOs in natural eclogites (Bascou *et al*., 2001, 2002; Mauler *et al*., 2001). The experimental results demonstrate that the observed omphacite LPOs could arise solely from dislocation creep in omphacite, removing the need to postulate complicated diffusion-based models. Previous work on polycrystalline omphacite has shown that both S- and L-type omphacite fabrics can be produced by combined slip systems of (100)[001], {110}[001] and $\{110\}1/2<110>$ (Zhang *et al*., 2006).

The results also show that S-type fabric and its mesoscopic foliation develop under conditions of axially-symmetric shortening whereas L-type fabric and its mesoscopic lineation develop under conditions of general strain, with L parallel to the greatest elongation. Because omphacite space group transformation is not involved during the experiments, it is concluded that the variation between S- and L-type omphacite fabric seen in nature arises from variation of the geometry and orientation of the finite strain ellipsoid, as would be expected from symmetry arguments (Paterson & Weiss, 1961). The control of fabric by strain and rotation rather than stress or crystallography is

clearly demonstrated by the simultaneous rotation of the L-maximum and the lineation defined by crystal elongation towards the shear plane with progressive strain in shear experiments. It is also consistent with the prediction of computer simulations and observations of high-temperature mantle eclogite xenoliths (Bascou *et al*., 2001, 2002; Ulrich & Mainprice, 2005).

Rutile deformation mechanism

Our results reveal a consistent LPO in rutile from experimentally deformed dry eclogite: [001] forms a girdle near the foliation plane and maxima of $<100>$ and {110} approximately parallel to foliation. This fabric is compatible with fabrics discovered in rutile of many natural eclogites suggesting a result of dislocation glide on {110}[001] (Mauler *et al*., 2001). This slip system has been observed to be active in laboratory experiments on rutile single crystals. The other operating slip system is the $\{101\}<101>$ slip system, which is less active with increase of temperature (Blanchin *et al*., 1990).

Quartz deformation mechanism

The deformation mechanism and LPO of quartz are often complicated because of it having a large number of available slip systems. The dominant slip systems in quartz vary significantly as a function of temperature, differential stress, strain rate and presence of water in the lattice and along grain boundaries (Tullis, 2002). Hirth & Tullis (1992) identified three regimes of dislocation creep in experimentally deformed quartz aggregates. It undergoes basal glide at low temperatures [slip along the (0001) plane in any of the 3 **a** directions], prismatic slip at moderate temperatures (slip along the prism planes in any of the 3 **a** directions), and **c**-slip at high temperatures (slip along the prism planes in the **c** direction).

This study provides insight into the quartz deformation mechanism at temperatures and pressures much higher than those previous studies. Quartz appears to be the weakest mineral in eclogite as suggested by its large grain aspect ratio after deformation. It is expected to develop strong high-temperature LPO (Hirth & Tullis, 1992). However, the results failed to provide evidence of strong fabric development. Instead, complicated and inconsistent quartz LPOs were observed. Similar phenomena are also observed in quartz from natural eclogites (Binns, 1967; Mauler *et al*., 2001). It has often been attributed to late static recrystallization and recovery processes during retrogression. It is not possible to use this effect to explain the quartz fabrics because the deformation experiments were conducted at constant temperature, pressure and strain rate conditions and then quenched to 300 °C in a few seconds. Because the same is seen in natural and experimental eclogites, it is concludes that this is a normal product of quartz deformation under this regime in which it is a minor phase distributed amongst much stronger phases. Clearly, several slip systems have been activated simultaneously in all or most quartz crystals, with different ones activated in crystals of different orientation. The implication is that the critical resolved shear stress becomes similar for many slip systems in quartz at high pressure.

ACKNOWLEDGEMENTS

We thank Z-M Jin, H. Jung and L. Dobrzhinetskaya for constructive discussions of experimental procedures, H. Jung for assistance with EBSD technique and F. Forgit for machining parts for the sample assemblies and general apparatus maintenance. The critical reviews and constructive comments by D. Mainprice and G. Godard are greatly appreciated. We also thank L. Dobrzhinetskaya for editorial review. This work was sponsored by the US National Science Foundation (Grant no. Ear#0003631 to H. W. Green).

REFERENCES

Aines, R. D. & Rossman, G. R., 1984. The water content of mantle garnet. *Geology*, **12,** 720–723.

Allen, F. M., Smith, B. K. & Buseck, P. R., 1987. Direct observation of dissociated dislocations in garnet. *Science*, **238,** 1623.

Ando, J., Fujino, K. & Takeshita, T., 1993. Dislocation microstructures in naturally deformed silicate garnets. *Physics of the Earth and Planetary Interiors*, **80,** 105–106.

Austrheim, H. & Boundy, T. M., 1994. Pseudotachylytes generated during seismic faulting and eclogitization of the deep crust. *Science*, **265,** 82–83.

Avé Lallement, H. G., 1978. Deformation of diopside and websterite. *Tectonophysics*, **48,** 1–27.

Bai, Q. & Green, H. W. II, 1998. Plastic flow of Mn_2GeO_4 I: toward a rheological model of the Earth's transition zone. In: *Properties of Earth and Planetary Materials at High Pressure and Temperature* (eds Manghnani, M. H. & Yagi, T.), *Geophysical Monograph*, **101,** 461–472.

Bascou, J., Barruol, G., Vauchez, A., Mainprice, D. & Egydio-Silva, M., 2001. EBSD-measured lattice-preferred orientations and seismic properties of eclogites. *Tectonophysics*, **342,** 61–80.

Bascou, J., Tommasi, A. & Mainprice, D., 2002. Plastic deformation and development of clinopyroxene lattice preferred orientations in eclogites. *Journal of Structural Geology*, **24,** 1357–1368.

Bell, D. R. & Rossman, G. R., 1992. Water in earth's mantle: the role of nominally anhydrous minerals. *Science*, **255,** 1391–1397.

Bell, D. R., Ihinger, P. D. & Rossman, G. R., 1995. Quantitative analysis of trace OH in garnet and pyroxenes. *American Mineralogist*, **80,** 465–474.

Binns, R. A., 1967. Barroisite-bearing eclogite from Naustdal, Song of Fjordane, Norway. *Journal of Petrology*, **8,** 349–371.

Bird, P., 1979. Continental delamination and the Colorado Plateau. *Journal of Geophysical Research*, **84,** 7561–7571.

Blanchin, M. G., Bursill, L. A. & Lafage, C., 1990. Deformation and microstructure of rutile. *Proceedings of the Royal Society of London*, **249,** 175–202.

Boland, J. N. & Tullis, T. E., 1986. Deformation behavior of wet and dry clinopyroxenite in the brittle to ductile transition region. In: *Mineral and Rock Deformation: Laboratory Studies – The Paterson Volume* (eds Hobbs, B. E. & Heard, H. C.), *Geophysical Monograph*, **36,** 35–49.

Boundy, T. M., Fountain, D. M. & Austrheim, H., 1992. Structural development and petrofabrics of eclogite facies shear zones, Bergen Arcs, western Norway: implications for deep crustal deformational processes. *Journal of Metamorphic Geology*, **10,** 127–146.

Brenker, F. E., Prior, D. J. & Müller, W. F., 2002. Cation ordering in omphacite and effect on deformation mechanism and lattice preferred prientation (LPO). *Journal of Structural Geology*, **24,** 1991–2005.

den Brok, B. & Kruhl, J. K., 1996. Ductility of garnet as an indicator of extremely high temperature deformation: discussion. *Journal of Structural Geology*, **18,** 1369–1373.

Buatier, M., van Roermund, H. L., Dury, M. R. & Lardeaux, J. M., 1991. Deformation and recrystallization mechanisms in naturally deformed omphacites from the Sesia-Lanzo zone: geophysical consequences. *Tectonophysics*, **195,** 11–27.

Bystricky, M. & Mackwell, S., 2001. Creep of dry clinopyroxene aggregates. *Journal of Geophysical Research*, **106,** 13443–13454.

Chopin, C., 1984. Coesite and pure pyrope in high-grade blueschists of the western Alps: a first record and some consequences. *Contributions to Mineralogy and Petrology*, **86,** 107–118.

Coleman, R. G. & Wang, X., eds, 1995. *Ultrahigh Pressure Metamorphism*. Cambridge University Press, New York.

Cordier, P., Ratteron, P. & Wang, Y., 1996. TEM investigation of dislocation microstructure of experimentally deformed silicate garnet. *Physics of the Earth and Planetary Interiors*, **97,** 121–131.

Dimanov, A., Lavie, M. P., Dreson, G., Ingrin, J. & Jaoul, O., 2003. Creep of polycrystalline anorthite and diopside. *Journal of Geophysical Research*, **108,** B1, 2061, doi:10.1029/2002JB001815.

Dobrzhinetskaya, L. F., Eide, E., Larsen, R. *et al*., 1995. Diamond in metamorphic rocks of the Western Gneiss Region in Norway. *Geology*, **23,** 597–600.

Dobrzhinetskaya, L. F., Schweinehage, R., Massonne, H. J. & Green, H. W., 2002. Silica precipitates in omphacite from eclogite at Alpe Arami, Switzerland: evidence of deep subduction. *Journal of Metamorphic Geology*, **20,** 481–492.

Doukhan, N., Sautter, V. & Doukhan, J. C., 1994. Ultradeep, ultra-mafic mantle xenoliths – transmission electron microscopy preliminary results. *Physics of the Earth and Planetary Interiors*, **82,** 195–207.

Ducea, M. & Saleeby, J., 1998. A case for delamination of the deep batholithic crust beneath the Sierra Nevada, California. *International Geology Review*, **40,** 78–93.

Godard, G., 1988. Petrology of some eclogites in the Hercynides: the eclogites from the Southern Armorican Massif, France. In: *Eclogites and Eclogite-Facies Rocks* (ed. Smith, D. C.), *Reviews of Petrology*, **12,** 451–510.

Godard, G., 2001. Eclogites and their geodynamic interpretations: a history. *Journal of Geodynamics*, **32,** 165–203.

Godard, G. & van Roermund, H. L. M., 1995. Deformation-induced clinopyroxene fabrics from eclogites. *Journal of Structural Geology*, **17,** 1425–1443.

Green, D. H., 1973. Experimental melting studies on a model upper mantle composition at high pressure under water-saturated and water-undersaturated conditions. *Earth and Planetary Science Letters*, **19,** 37–53.

Green, H. W. II, 2005. Psychology of a changing paradigm: 40 + years of high-pressure metamorphism. *International Geology Review*, **47,** 439–456.

Green, H. W. & Borch, R. S., 1987. The pressure dependence of creep. *Acta Metallurgica*, **35,** 1301–1305.

Green, H. W., Dobrzhinetskaya, L. & Bozhilov, K. N., 2000. Mineralogical and experimental evidence for very deep exhumation from subduction zones. *Journal of Geodynamics*, **30,** 61–76.

Griggs, D. T., 1967. Hydrolytic weakening of quartz and other silicates. *Geophysical Journal of the Royal Astronomical Society*, **14,** 19–31.

Griggs, D. T. & Blacic, J. D., 1965. Quartz: anomalous weakness of synthetic crystals. *Science*, **147,** 292–295.

Hacker, B. R. & Liou, J. G., eds, 1998. *When Continents Collide: Geodynamics and Geochemistry of Ultrahigh-Pressure Rocks*. Kluwer Academic Publishers, the Netherlands.

Hacker, B. R., Peacock, S. M., Abers, G. A. & Holloway, S. D., 2003. Subduction factory – 2. Are intermediate-depth earthquakes in subducting slabs linked to metamorphic dehydration reactions?. *Journal of Geophysical Research*, **108,** NO. B1, 2030, doi:10.1029/2001JB001129.

Hammer, V. M. F. & Beran, A., 1991. Variations in the OH concentration of rutiles from different geological environments. *Mineralogy and Petrology*, **48,** 257–268.

Häuy, R. J., 1822. *Traité de Minéralogie (Second edition), revue, corrigée, considérablement augmentée par l'auteur*. Bachelier et Huzard, Paris.

Helmstaedt, H., Anderson, D. L. & Gavasci, A. T., 1972. Petrofabric studies of eclogite, spinel websterite, and spinel-lherzolite xenoliths from kimberlite-breccia pipes in southeastern Utah and northeastern Arizona. *Journal of Geophysical Research*, **77,** 4350–4365.

Hirth, G. & Tullis, J., 1992. Dislocation creep regimes in quartz aggregates. *Journal of Structural Geology*, **14,** 145–159.

Ingrin, J. & Madon, M., 1995. TEM observations of several spinel-garnet assemblies: toward the rheology of the transition zone. *Terra Nova*, **7,** 509–515.

Ingrin, J. & Skogby, H., 2000. Hydrogen in nominally anhydrous upper-mantle minerals: concentration levels and implications. *European Journal of Mineralogy*, **12,** 543–570.

Ingrin, J., Doukhan, N. & Doukhan, J. C., 1991. High-temperature deformation of diopside single crystals: 2, transmission electron microscopy investigation of the defect microstructures. *Journal of Geophysical Research*, **96,** 14287–14297.

Ji, S. & Martignole, J., 1994. Ductility of garnet as an indicator of extremely high temperature deformation. *Journal of Structural Geology*, **16,** 985–996.

Ji, S., Saruwatari, K., Mainprice, D., Wirth, R., Xu, Z. & Xia, B., 2003. Microstructure, petrofabrics and seismic properties of ultrahigh-pressure eclogites from Sulu region, China: implications for rheology of subducted continental crust and origin of mantle reflections. *Tectonophysics*, **370,** 49–76.

Jin, Z., Zhang, J., Green, H. W. & Jin, S., 2001. Eclogite rheology: implications for subducted lithosphere. *Geology*, **29,** 667–670.

Jung, H. & Karato, S., 2001. Water-induced fabric transitions in olivine. *Science*, **293,** 1460–1463.

Jung, H., Green, H. W. & Dobrzhinetskaya, L. F., 2004. Intermediate-depth earthquake faulting by dehydration embrittlement with negative volume change. *Nature*, **428,** 545–549.

Karato, S., Wang, Z., Liu, B. & Fujino, K., 1995. Plastic deformation of garnets: systematics and implications for the rheology of the mantle transition zone. *Earth and Planetary Science Letters*, **130,** 13–30.

Katayama, I. & Nakashima, S., 2003. Hydroxyl in clinopyroxene from the deep subducted crust: evidence for H_2O transport into the mantle. *American Mineralogists*, **88,** 229–234.

Kay, R. W. & Kay, S. M., 1993. Delamination and delamination magmatism. *Tectonophysics*, **219,** 177–189.

van Keken, P. E., Karato, S. & Yuen, D. A., 1996. Rheological control of oceanic crust separation in the transition zone. *Geophysical Research Letters*, **23,** 1821–1824.

Kirby, S. H. & Kronenberg, A. K., 1984. Deformation of clinopyroxenite: Evidence for a transition in flow mechanisms and semibrittle behavior. *Journal of Geophysical Research*, **89,** 3177–3192.

Kirby, S. H., Engdahl, E. R. & Denlinger, R. P., 1996. Intermediate-depth intraslab earthquakes and arc volcanism as physical expressions of crustal and uppermost mantle metamorphism in subducting slabs. In: *Subduction Top to Bottom* (eds Bebou, G. E., Scholl, D. W., Kirby, S. H. & Platt, J. P.), *Geophysical Monograph*, **96,** 195–214.

Kleinschrodt, R. & Duyster, J. P., 2002. HT-deformation of garnet: an EBSD study on granulites from Sri Lanka, India and the Ivrea Zone. *Journal of Structural Geology*, **24,** 1829–1844.

Kleinschrodt, R. & McGrew, A. J., 2000. Garnet plasticity in the lower continental crust: implications for deformation mechanisms based on microstructures and SEM electron channeling pattern analysis. *Journal of Structural Geology*, **22,** 795–809.

Langer, K., Robarick, E., Sobolev, N. V., Shatsky, V. S. & Wang, W., 1993. Single-crystal spectra of garnets from diamondiferous high-pressure metamorphic rocks from Kazakhstan: indications for OH^-, H_2O, and FeTi charge transfer. *European Journal of Mineralogy*, **5,** 1091–1100.

Mackwell, S. J., 1991. High-temperature rheology of enstatite: implications for creep in the mantle. *Journal of Geophysical Research*, **96,** 14277–14286.

Madon, M. & Poirier, J. P., 1980. Dislocations in spinel and garnet high-pressure polymorphs of olivine and pyroxene: implications for mantle rheology. *Science*, **207,** 66–68.

Mainprice, D., Bascou, J., Cordier, P. & Tommasi, A., 2004. Crystal preferred orientations of garnet: comparison between numerical simulations and electron back-scattered diffraction (EBSD) measurements in naturally deformed eclogites. *Journal of Structural Geology*, **26,** 2089–2102.

Mauler, A., Godard, G. & Kunze, K., 2001. Crystallographic fabrics of omphacite, rutile and quartz in Vendée eclogite (Armorican Massif, France): Consequences for deformation mechanisms and regimes. *Tectonophysics*, **342,** 81–112.

Paterson, M. S. & Weiss, L. E., 1961. Symmetry concepts in the structural analysis of deformed rocks. *Geological Society of America Bulletin*, **72,** 841–882.

Philippot, P. & van Roermund, H. L. M., 1992. Deformation processes in eclogitic rocks: evidence for the rheological delamination of the oceanic crust in deeper levels of subduction zones. *Journal of Structural Geology*, **14,** 1059–1077.

Piepenbreier, D. & Stöckhert, B., 2001. Plastic flow of omphacite in eclogites at temperatures below 500 °C-implications for interplate coupling in subduction zones. *International Journal of Earth Sciences*, **90,** 197–210.

Poirier, J. P., 1985. *Creep of Crystals*. Cambridge University Press, New York.

Poli, S. & Schmidt, M. W., 2002. Petrology of subducted slabs. *Annual Review of Earth and Planetary Sciences*, **30,** 207–235.

Prior, D. J., 1999. Problems in determining the orientations of crystal misorientation axes for small angular misorientations using electron backscatter diffraction in the SEM. *Journal of Microscopy*, **195,** 217–225.

Prior, D. J., Wheeler, J., Brenker, F. E., Harte, B. & Matthews, M., 2000. Crystal plasticity of natural garnet: new microstructural evidence. *Geology*, **28,** 1003–1006.

Raleigh, C. B. & Paterson, M. S., 1965. Experimental deformation of serpentinite and its tectonic implications. *Journal of Geophysical Research*, **70,** 3965–3985.

Raleigh, C. B., Kirby, S. H., Cater, N. L. & Ave'Lallemant, H. G., 1971. Slip and the clinoenstatite transformation as competing rate processes in enstatite. *Journal of Geophysical Research*, **76,** 4011–4022.

Raterron, P. & Jaoul, O., 1991. High-temperature deformation of diopside single crystal, 1, Mechanical data. *Journal of Geophysical Research*, **96,** 14277–14286.

Raterron, P., Doukhan, N., Jaoul, O. & Doukhan, J. C., 1994. High temperature deformation of diopside: IV. Predominance of 110 glide above 1000 °C. *Physics of the Earth and Planetary Interiors*, **82,** 209–222.

Ringwood, A. E., 1991. Phase transformations and their bearing on the constitution and dynamics of the mantle. *Geochimica et Cosmochimica Acta*, **55,** 2083–2110.

Ringwood, A. E. & Green, D. H., 1966. An experimental investigation of the gabbro-eclogite transformation and some geophysical implications. *Tectonophysics*, **3,** 383–427.

van Roermund, H. L. M., 1983. Petrofabics and microstructures of omphacites in a high temperature eclogite from the Swedish Caledonides. *Bulletin of Mineralogy*, **106,** 709–713.

van Roermund, H. L. M. & Boland, J. N., 1981. The dislocation substructures of natural deformed Omphacite. *Tectonophysics*, **78,** 403–418.

Ross, J. V. & Nielsen, K. C., 1978. High-temperature flow of wet polycrystalline enstatite. *Tectonophysics*, **44,** 233–261.

Rummel, F., 1969. Studies of time-dependant deformation of some granite and eclogite rock samples under uniaxial, constant compressive stress and temperatures up to 400 deg C. *Zeitschr Geophysik*, **35,** 17–42.

Sacks, P. E. & Secor, D. T., 1990. Delamination in collisional orogens. *Geology*, **18,** 999–1002.

Seber, D., Barazangi, M., Ibebrahim, A. & Demnati, A., 1996. Geophysical evidence for lithospheric delamination beneath the Alboran Sea and Rif-Betic mountains. *Nature*, **379,** 785–790.

Smith, D. C., 1984. Coesite in clinopyroxene in the Caledonides and its implications for geodynamics. *Nature*, **310,** 641–644.

Smith, D. C., ed., 1988. *Eclogites and Eclogite-Facies Rocks*. Developments in Petrology, 12, Elsevier, Amsterdam.

Smyth, J. R., Bell, D. R. & Rossman, R. G., 1991. Incorporation of hydroxyl in upper-mantle clinopyroxenes. *Nature*, **351,** 732–735.

Sobolev, N. V. & Shatsky, V. S., 1990. Diamond inclusions in garnets from metamorphic rocks. *Nature*, **343,** 742–746.

Song, S., Zhang, L., Chen, J., Liou, J. G. & Niu, Y., 2005. Sodic amphibole exsolutions in garnet from garnet-peridotite, North Qaidam UHPM belt, NW China: implications for ultradeep-origin and hydroxyl defects in mantle garnets. *American Mineralogist*, **90,** 814–820.

Stöckhert, B. & Renner, J., 1998. Rheology of crustal rocks at ultrahigh pressure. In: *When Continents Collide: Geodynamics and Geochemistry of Ultrahigh-Pressure Rocks* (eds Hacker, B. R. & Liu, J. G.), pp. 57–95. Kluwer Academic Publishers, the Netherlands.

Storey, G. D. & Prior, D. J., 2005. Plastic deformation and recrystallization of garnet: a mechanism to facilitate diffusion creep. *Journal of petrology*, **46,** 2593–2613.

Su, W., Ji, Z. P., You, Z. D., Cong, B., Ye, K. & Zhong, Z., 2004. Distribution of hydrous components in jadeite of the Dabie Mountains. *Earth and Planetary Science Letters*, **222,** 85–100.

Terry, M. P. & Heidelbach, F., 2004. Superplasticity in garnet from eclogite facies shear zones in the Haram Gabbro, Haramsøya, Norway. *Geology*, **32,** 281–284.

Terry, M. P. & Heidelbach, F., 2006. Deformation-enhanced metamorphic reactions and the rheology of high-pressure shear zones, Western Gneiss Region, Norway. *Journal of Metamorphic Geology*, **24,** 3–18.

Tingle, T. N., Green, H. W., Young, T. E. & Koczynski, T. A., 1993. Improvements to Griggs-type apparatus for mechanical testing at high pressures and temperatures. *Pageoph*, **141,** 523–543.

Tullis, J., 2002. Deformation of granitic rocks: experimental studies and natural examples. In *Plasticity of Minerals and Rocks* (eds Karato, S. & Wenk, H.), *Reviews in Mineralogy and Geochemistry*, **51,** 51–95.

Ulrich, S. & Mainprice, D., 2005. Does cation ordering in omphacite influence development of lattice-preferred orientation? *Journal of Structural Geology*, **27,** 419–431.

Vöegele, V., Ando, J. I., Cordier, P. & Liebermann, R. C., 1998. Plastic deformation of silicate garnets I. High-pressure experiments. *Physics of the Earth and Planetary Interiors*, **108,** 305–318.

Wang, Z. & Ji, S., 1999. Deformation of silicate garnets: Brittle-ductile transition and its geological implications. *Canadian Mineralogist*, **37,** 525–541.

Wang, Z. & Ji, S., 2000. Diffusion creep of fine-grained garnetite: implications for the flow strength of subducting slabs. *Geophysical Research Letters*, **27,** 2333–2336.

Warner, M., Morgan, J., Barton, P., Jones, K., Barton, P. & Morgan, P., 1996. Seismic reflections from the mantle represent relict subduction zones within the continental lithosphere. *Geology*, **24,** 39–42.

Wenk, H. R., Cont, L., Xie, Y., Lutterotti, L., Ratschbacher, L. & Richardson, J., 2001. Rietveld Texture analysis of Dabie Shan eclogite from TOF neutron diffraction spectra. *Journal of Applied Crystallography*, **34,** 442–453.

Withers, A. C., Wood, B. J. & Carro11, M. R., 1998. The OH content of pyrope at high pressure. *Chemical Geology*, **147,** 161–l7l.

Xu, S., Okay, A., Ji, S. *et al*., 1992. Diamond from the Dabie Shan metamorphic rocks and its implication for tectonic setting. *Science*, **256,** 80–82.

Zhang, J. & Green, H. W., 2006. On the deformation of UHP eclogite: from laboratory to nature. *International Geology Review*, in press.

Zhang, J., Green, H. W., Bozhilov, K. & Jin, Z.-M., 2004. Faulting induced by precipitation of water at grain boundaries in hot subducting oceanic crust. *Nature*, **428,** 633–636.

Zhang, J., Green, H. W. & Bozhilov, K., 2006. Rheology of omphacite at high temperature and pressure and significance of its lattice preferred orientations. *Earth and Planetary Science Letters*, **246,** 432–443.

Received 23 March 2006; revision accepted 25 September 2006.